Computer Physics Communications 182 (2011) 1391–1401

Contents lists available at ScienceDirect

Computer Physics Communications

www.elsevier.com/locate/cpc

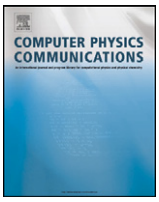

Matrix algorithms for solving (in)homogeneous bound state equations

M. Blank, A. Krassnigg *

Institut für Physik, Universität Graz, Universitätsplatz 5, 8010 Graz, Austria

ARTICLE INFO

Article history:
Received 16 September 2010
Received in revised form 11 February 2011
Accepted 6 March 2011
Available online 17 March 2011

Keywords:
Bethe–Salpeter equation
Faddeev equation
Integral equation
Solution methods

ABSTRACT

In the functional approach to quantum chromodynamics, the properties of hadronic bound states are accessible via covariant integral equations, e.g. the Bethe–Salpeter equation for mesons. In particular, one has to deal with linear, homogeneous integral equations which, in sophisticated model setups, use numerical representations of the solutions of other integral equations as part of their input. Analogously, inhomogeneous equations can be constructed to obtain off-shell information in addition to bound-state masses and other properties obtained from the covariant analogue to a wave function of the bound state. These can be solved very efficiently using well-known matrix algorithms for eigenvalues (in the homogeneous case) and the solution of linear systems (in the inhomogeneous case). We demonstrate this by solving the homogeneous and inhomogeneous Bethe–Salpeter equations and find, e.g. that for the calculation of the mass spectrum it is as efficient or even advantageous to use the inhomogeneous equation as compared to the homogeneous. This is valuable insight, in particular for the study of baryons in a three-quark setup and more involved systems.

1. Introduction

The underlying quantum field theory of the strong interaction in the standard model of elementary particle physics is quantum chromodynamics (QCD), a non-abelian gauge theory which deals with elementary degrees of freedom called quarks and gluons [1]. A remarkable feature of QCD is asymptotic freedom, which means that the running coupling of the theory is small in the high-energy regime [2–4]. There, perturbation theory can be applied, and perturbative QCD has been well established in the high-energy domain, (e.g. [5] and references therein). At low energies, however, perturbation theory is no longer applicable, since the value of the running coupling increases to the order of 1. Since bound states are intrinsically nonperturbative, corresponding methods have been developed and used to investigate hadrons, the bound states of quarks and gluons. We eclectically list a few references regarding constituent quark models [6–10], effective field theories [11–13], lattice-regularized QCD [14–19], QCD sum rules [20–25], and the renormalization-group approach to QCD [26,27] (always see also references therein).

Another remarkable property closely related to bound states is the so-called confinement of quarks and gluons. It entails that only objects like hadrons, where the color charges carried by the elementary degrees of freedom are combined to a color-neutral state, can be observed directly. While in constituent-quark models confinement is usually implemented via potential terms of an infinitely rising nature (of, e.g., harmonic-oscillator or linear type), in QCD the particularities are more delicate (for a recent review of the problems surrounding quark confinement, see e.g. [28]). In a quantum field theoretical setup, as we use it here, confinement is tied to the properties of the fundamental Green functions of the theory.

In the present work, we employ the Dyson–Schwinger-equation (DSE) approach to QCD. The DSEs are the covariant and nonperturbative continuum equations of motion in quantum field theory. They constitute an infinite set of coupled and in general nonlinear integral equations for the Green functions of the quantum field theory under consideration. There are several extensive reviews on the subject that focus on different aspects of DSEs, like fundamental Green functions [29–31], bound-state calculations [32,33] and applications of the formalism, e.g. to QCD at finite temperature and density [34]. Bound states are studied in this approach with the help of covariant equations embedded in the system of DSEs. In particular, the Bethe–Salpeter equation (BSE) [35,36] is used for two-body problems such as mesons [37–39] and covariant Faddeev-type equations [40] are used for three-body problems such as baryons [41,42].

Ideally, one could obtain a self-consistent simultaneous solution of all DSEs, which would be equivalent to a solution of the underlying quantum field theory. While in investigations of certain aspects of the theory such an approach is successful (see, e.g. [43,44] and references therein), numerical studies of hadrons necessitate a truncation of this infinite tower of equations.

* Corresponding author.
E-mail addresses: martina.blank@uni-graz.at (M. Blank), andreas.krassnigg@uni-graz.at (A. Krassnigg).

0010-4655
doi:10.1016/j.cpc.2011.03.003

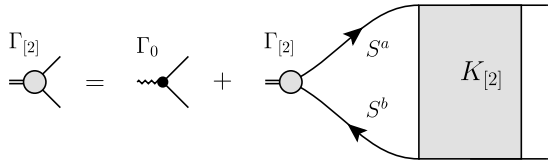

Fig. 1. The inhomogeneous vertex BSE, Eq. (1).

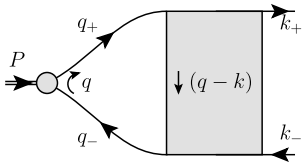

Fig. 2. Momentum flow of the loop-diagram present in Eqs. (1) and (2).

Given such a truncation, the mass spectrum of the system under consideration can be investigated by either directly solving the relevant covariant bound-state equation such as the homogeneous quark–anti-quark BSE for a meson or investigating the pole structure of the solution of the corresponding inhomogeneous vertex BSE. Subsequently, the corresponding covariant amplitudes can be used to compute further observables of the bound states found in the system. In the past, on-shell information about bound states has been almost exclusively obtained via the homogeneous BSE for mesons as well as baryons. The inhomogeneous vertex equations on the other hand were used for studies of, e.g., the quark photon vertex and correlation functions. Recently, it was shown how it is also possible to use an inhomogeneous vertex equation to study on-shell properties of bound states, such as leptonic decay constants [45].

Prominent examples for hadron properties studied in such a setup in rainbow-ladder truncation (which is specified further below) include leptonic decay constants [46–48], hadronic decays [49,50], and electromagnetic properties of both mesons [51–55] and baryons [56–61]. Improvements to this truncation have been considered in the past and studies in this direction are under way [62–67]. What we discuss in the present work is most easily exemplified in a simple truncation, but becomes more important — and thus relevant — with any kind of increasing numerical effort necessitated by either a more involved truncation or the study of a system of more than two constituents.

The paper is organized as follows: in Section 2 we collect the necessary formulae regarding covariant integral equations as they are obtained in the DSE approach to QCD. Section 3 details the discretization of the integrals and the general numerical setup. Section 4 contains numerical solution strategies for both the homogeneous and inhomogeneous types of equations. In Section 5 we apply the methods described to solve the homogeneous and inhomogeneous BSEs for pseudoscalar mesons in rainbow-ladder truncation and analyze the efficiency of the algorithms. Further quantum numbers are discussed in Section 6. Conclusions and an outlook indicating both immediate and further possible applications of the strategies described herein are offered in Section 7.

All calculations are performed in Euclidean momentum space.

2. Structure of covariant bound-state equations

In order to study mesons as bound states of quarks, anti-quarks and gluons in the DSE approach to QCD, one can consider general vertices connecting (anti-)quarks to objects carrying the appropriate quantum numbers as demanded by the respective superselection rules. These vertices are the so-called (inhomogeneous) Bethe–Salpeter amplitudes (BSAs), denoted by $\Gamma_{[2]}(k,P)$, which describe a two-particle system, denoted by the subscript [2], with total momentum P and relative momentum k of the constituents. The inhomogeneous BSA satisfies the inhomogeneous (vertex) BSE,

$$\Gamma_{[2]}(k,P) = \Gamma_0(k,P) + \int_q K_{[2]}(k,q,P) S^a(q_+) \Gamma_{[2]}(q,P) S^b(q_-). \tag{1}$$

Here $\Gamma_0(k,P)$ is a renormalized current (cf. [68]) with the quantum numbers of the system which acts as a driving term, and $S^{a,b}(q_\pm)$ denote the renormalized dressed (anti-)quark propagators. As opposed to bare propagators, they are obtained as solutions of the quark DSE, Eq. (6). Together with the renormalized quark–anti-quark scattering kernel $K_{[2]}(k,q,P)$ the propagators provide the input necessary to solve the BSE. This equation is formulated in Euclidean space, and the four-dimensional momentum integration (including a translationally invariant regularization) is given by $\int_q = \int \frac{d^4q}{(2\pi)^4}$. A graphical representation of Eq. (1) is given in Fig. 1, where the arrows denote dressed-quark propagators (analogously in Figs. 3 and 4). The momentum flow (detailed in Fig. 2) is defined such that the total momentum P is given by the difference of the (anti-)quark momenta $q_\pm = q \pm \eta_\pm P$. $\eta_\pm$ represents the momentum partitioning parameters, which satisfy $\eta_+ + \eta_- = 1$. The relative momentum q of the BSA is therefore given by $q = \eta_- q_+ + \eta_+ q_-$. On the left-hand side of Eqs. (1) and (2) the relative momentum is denoted by k.

The solution of (1), $\Gamma_{[2]}(k,P)$, contains both off-shell and on-shell information about the states in a channel with the quantum numbers under consideration, which are fixed via the construction of $\Gamma_0(k,P)$ and $\Gamma_{[2]}(k,P)$. In particular, $\Gamma_{[2]}(k,P)$ has poles[1] whenever the total-momentum squared corresponds to the square of a bound-state mass in this channel (e.g. [69] and references therein). If there exists a bound state and the corresponding on-shell condition, in Euclidean space $P^2 = -M^2$, is met, the properties of the bound state are described by the pole residues of Eq. (1). These residues, the homogeneous BSAs $\Gamma_{[2h]}(k,P)$, can be obtained from the corresponding homogeneous BSE,

$$\Gamma_{[2h]}(k,P) = \int_q K_{[2]}(k,q,P) S^a(q_+) \Gamma_{[2h]}(q,P) S^b(q_-), \tag{2}$$

depicted in Fig. 3. While the inhomogeneous BSE needs to be renormalized, this is not the case for the homogeneous BSE. Instead, the physical on-shell amplitudes satisfy a "canonical" normalization condition (see, e.g., [46])

$$\begin{aligned} 2P_\mu &= \mathrm{Tr}\Bigg[\int_q \left(\frac{\partial}{\partial Q_\mu} S^a(q+\eta_+ Q) \right) \bar{\Gamma}_{[2h]}(q,-P) S^b(q_-) \Gamma_{[2h]}(q,P) \\ &\quad + \int_q S^a(q_+) \bar{\Gamma}_{[2h]}(q,-P) \left(\frac{\partial}{\partial Q_\mu} S^b(q-\eta_- Q) \right) \Gamma_{[2h]}(q,P) \\ &\quad + \int_q \int_k S^a(q_+) \bar{\Gamma}_{[2h]}(q,-P) S^b(q_-) \\ &\quad \times \left(\frac{\partial}{\partial Q_\mu} K_{[2]}(q,k,Q) \right) S^a(p_+) \Gamma_{[2h]}(k,P) S^b(k_-) \Bigg]_{Q=P}, \end{aligned} \tag{3}$$

where $\bar{\Gamma}_{[2h]}(q,-P)$ refers to the charge-conjugate amplitude, defined as

[1] It should be noted that this formalism is also applicable to resonances, where the pole in $\Gamma_{[2]}(k,P)$ is at a complex value of P^2 instead of a real value, which leads to a peak-structure for $P^2 \in \mathbf{R}$.

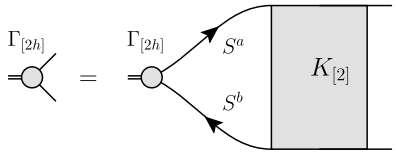

Fig. 3. The homogeneous BSE, Eq. (2).

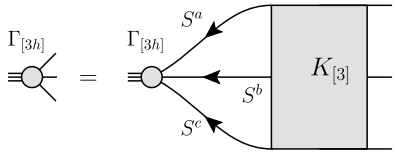

Fig. 4. The homogeneous equation for a three-body bound state (covariant Faddeev equation), Eq. (5).

$$\bar{\Gamma}_{[2h]}(q,-P) = \left[C\Gamma_{[2h]}(-q,-P)C^{-1}\right]^t, \tag{4}$$

using the charge-conjugation matrix $C = \gamma_2\gamma_4$ and denoting the matrix transpose by the superscript t.

For Baryons, an analogous construction can be made, where the homogeneous equation for the on-shell amplitude is a covariant three-quark equation often referred to as a covariant Faddeev equation [42,70,71], which may be written as

$$\Gamma_{[3h]}(k_1,k_2,P) = \int_{q_1,q_2} S^a(p_1)S^b(p_2)S^c(p_3) \times K_{[3]}(k_1,k_2,q_1,q_2,P)\Gamma_{[3h]}(q_1,q_2,P), \tag{5}$$

and a pictorial representation is given in Fig. 4. Here, the kernel $K_{[3]}(k_1,k_2,q_1,q_2,P)$ subsumes all interactions of the three quarks with the individual momenta p_i, $i=1,2,3$, and the bound state is described by the covariant three-quark on-shell amplitude $\Gamma_{[3h]}(k_1,k_2,P)$, which depends on the total momentum P as well as two relative (Jacobi) momenta k_1 and k_2. Note that this equation contains an integral over two momenta, namely q_1 and q_2, thus inflating the size of the problem in terms of a numerical setup.

While in this work we will focus on the solution of equations such as (1) or (2), a note on the construction of the interaction kernels K and the origin of the quark propagators S as inputs in these equations is in order. The propagators are the solutions of the quark DSE or gap equation,

$$S^{-1} = S_0^{-1} + \Sigma, \tag{6}$$

where S_0 is the bare quark propagator and the term Σ represents the self energy, which in turn depends on the dressed quark propagator S. Therefore, the DSE has to be solved self-consistently. However, the building blocks of Σ are not known exactly, such that a solution of Eq. (6) usually requires at least some modeling or assumptions, as does the construction of the quark–anti-quark scattering kernel K.

As a guideline, one can use the Ward–Takahashi- and/or Slavnov–Taylor identities, e.g. [29,30], which are satisfied by the Green functions of QCD in addition to the DSEs. These relate certain Green functions among each other and provide guidance or even constraints in many cases, if one is to use a truncation and wants to make a consistent Ansatz for $K_{[2]}$ and Σ. For light-hadron physics, the axial-vector Ward–Takahashi identity is of particular interest, since it encodes the chiral symmetry of QCD with massless quarks as well as its dynamical breaking (see, e.g. [46,68] for details). In other words, satisfaction of this identity guarantees that the properties of the pion, the lightest hadron and would-be Goldstone boson of dynamical chiral symmetry breaking, follow the expected pattern, e.g. the pion mass vanishes in the chiral limit, and leads to a generalized Gell-Mann–Oakes–Renner relation valid for all pseudoscalar mesons [68,72]. A particularly successful example of such a truncation is the rainbow-ladder truncation of the DSE-BSE system, which satisfies the axial-vector Ward–Takahashi identity. It is explained in more detail below, since we use it for our illustrative calculations. Beyond rainbow-ladder truncation, satisfaction of this identity can be achieved on more general terms and has been implemented throughout light-hadron studies of the past years in this approach, e.g. [62–66,73–75].

More concretely, the satisfaction of this identity leads to a close relation of the interaction kernel $K_{[2]}$ in the quark–anti-quark BSE and the quark self-energy present in the DSE of the quark propagator, the QCD gap equation. The consistent use of such related kernels in the BSE and the gap equation provides the proper input for the BSE in terms of the quark propagators S as solutions of the symmetry-preserving version of the gap equation. This consistency can be maintained also in numerical studies with high accuracy. In the following we always assume that the gap equation has been solved with the appropriate self-energy to match $K_{[2]}$ and that the resulting quark propagator S is known numerically.

In our Euclidean-momentum-space setup, the metric is given by $g_{\mu\nu} = \delta_{\mu\nu}$, with the corresponding consequences for the Clifford algebra of the Dirac γ matrices. A scalar product such as, e.g., $\gamma\cdot q$ in Eqs. (21) to (24) then denotes $\gamma\cdot q := \sum_{i=1,4}\gamma_i q_i$. Thus, the (timelike) total momentum of the system P has $P^2 < 0$ and the on-shell condition reads $P^2 = -M^2$, where M is the mass of the bound state. As a result, in a bound state equation set up in the system's rest frame, the real momentum-integration variables and the imaginary total on-shell momentum of the bound state are combined in the (anti-)quark momenta $q_\pm$ and q_1, q_2, q_3 to complex four-vectors. As a consequence, in general also the squares of the quark momenta are complex. In the meson BSE, for example, the propagator is needed in a parabolic region in the complex plane defined by $q_\pm^2$. Over the past years reliable numerical approaches to this problem have been developed and the required computations are well under control (for more details see [76–78]).

In this way, with the specification of the truncation used, one both decides the structure of the interaction kernel and obtains the quark propagator consistent with this kernel.

3. Numerical representation

The first step towards a numerical representation of Eqs. (1), (2), and (5) is the analysis of the Lorentz and Dirac structure of the respective amplitudes. This structure is a result of the particular representation of the symmetry properties of the state under consideration under the Lorentz group, including the state's parity and spin. Therefore, the amplitudes are decomposed into Lorentz-covariant parts T_i and Lorentz-invariant parts F^i, respectively, reading

$$\Gamma = \sum_{i=1}^{N} T_i F^i, \tag{7}$$

where the number of terms N as well as the tensor structure of the T_i and Γ depend on the quantum numbers of the state and all arguments have been suppressed for simplicity. The T_i are usually referred to as *covariants*, whereas we call the F^i the *components* of the amplitude Γ. The T_i represent a basis for the bound state, and one is — to some extent — free to choose the details thereof.

To be more concrete, we consider the case of two spin-1/2 fermions (the quark and anti-quark) in more detail, which are combined to a boson with total spin J and parity P. As a result one obtains a 4×4-matrix structure with the correct Lorentz-transformation properties for a state of spin J and parity P, see e.g. [37]. Consequently one has, in addition to the total momentum P^μ and the relative momentum q^μ between the constituents,

another four vector γ^μ of Dirac matrices to construct the elements of the BSA. The various combinations of the momenta and γ^μ correctly encode the angular momentum structures, i.e. the contributions of (anti-)quark spin and orbital angular momentum. The parity of the state is encoded in appropriate factors of γ_5 multiplying these structures.

A scalar quark–anti-quark BSA for example contains all possible Lorentz-scalar combinations of the three four-vectors P, q, and γ (the actual construction is given below for the pseudoscalar quantum numbers in Eqs. (21)–(24)). For the moment we note that while Γ and the T_i in Eq. (7) in the two-body case depend on the three four-vectors P, q, and γ as such (which we denote by semicolons between arguments of an expression), the components, being Lorentz- and Dirac-scalars, can only depend on scalar products of the momenta involved, i.e. P^2, q^2, and $q\cdot P$. Thus, writing arguments explicitly, Eq. (7) reads

$$\Gamma_{[2]}(\gamma;q;P)=\sum_{i=1}^{N}T_i(\gamma;q;P)F^i\big(P^2,q^2,q\cdot P\big), \tag{8}$$

where again the tensor structure of the T_i (and correspondingly Γ) was not denoted explicitly, since it is irrelevant to the following argument.

At this point, we would like to note that the structure of the covariants T_i does not determine all quantum numbers of the quark–anti-quark system. For constituents of equal masses, the homogeneous amplitude is an eigenstate of the operation of charge conjugation defined in Eq. (4), thus defining the quantum number of charge-conjugation parity (C-parity), $C=\pm1$. This determines the symmetry properties of the components with respect to $q\cdot P$, such that in this case a restriction of the symmetry of the components allows to select either $C=+1$ or $C=-1$. Here, however, we consider a general dependence on $q\cdot P$, such that the methods described here are also applicable in the case of constituents of unequal masses, where C-parity is not well-defined.

For numerical convenience, we use a basis that is orthonormal, meaning the covariants satisfy

$$\mathrm{Tr}(T_i\cdot T_j)=\delta_{i,j}, \tag{9}$$

which also defines a generalized scalar product on the space of 4×4 matrices (any occurring Lorentz indices are understood to be summed over here). Note that, for a set of covariants which is neither orthogonal nor normalized, the following step is more involved and we detail it in Appendix B. If one uses the decomposition (7), the bound state equations (1), (2), and (5) can be rewritten as coupled integral equations of the components depending on the scalar products of the momenta via the corresponding projections on the basis T_i.

More concretely, we consider the integrand in, e.g. the (in-)homogeneous BSE,

$$K_{[2]}(\gamma;k;q;P)S^a(\gamma;q;P)\Gamma_{[2]}(\gamma;q;P)S^b(\gamma;q;P). \tag{10}$$

The amplitude $\Gamma_{[2]}(\gamma;q;P)$ is expanded in the chosen Dirac basis $T_j(\gamma;q;P)$ and the result is projected on $T_i(\gamma;k;P)$. Doing so, one obtains a matrix structure in the space of covariants, and Eq. (10) can be written as a matrix–vector multiplication in this space involving the BSE *kernel matrix* $K^i_j(k;q;P)$:

$$\begin{aligned}&K^i_j(k;q;P)F^j\big(P^2,q^2,q\cdot P\big)\\&\quad=\mathrm{Tr}\big[T_i(\gamma;k;P)K_{[2]}(\gamma;k;q;P)S^a(\gamma;q;P)\\&\qquad\times T_j(\gamma;q;P)S^b(\gamma;q;P)\big]F^j\big(P^2,q^2,q\cdot P\big),\end{aligned} \tag{11}$$

where the sum over the repeated index j is implied.

The index j of the components $F^j(P^2,q^2,q\cdot P)$ can thus be viewed as a vector index, which has to be contracted with the corresponding index of the kernel matrix $K^i_j(k;q;P)$. Note that this procedure, although exemplified here for the case of the quark–anti-quark system, is completely general, i.e., it applies to three-body systems such as baryons as well and is valid for any choice of the interaction kernel K.

The next step is to make the dependence on the continuous momentum variables P^2, q^2, and $q\cdot P$ numerically accessible. To achieve this, we apply the so-called Nyström or quadrature method (cf. [79, Chapter 4]), which amounts to replacing an integral by a sum over suitable quadrature weights and points and neglecting the error term. Applying this method discretizes the integration variables, and consequently also the momentum dependence on the left-hand side. The homogeneous and the inhomogeneous integral equations can then be written as matrix equations in the covariants and the discretized momenta and read

$$F^{i,\mathcal{P}}_{[h]}=K^{i,\mathcal{P}}_{j,\mathcal{Q}}F^{j,\mathcal{Q}}_{[h]} \tag{12}$$

in the homogeneous case, and

$$F^{i,\mathcal{P}}=F^{i,\mathcal{P}}_0+K^{i,\mathcal{P}}_{j,\mathcal{Q}}F^{j,\mathcal{Q}} \tag{13}$$

in the inhomogeneous case. The indices i,j label the components, the multi-indices $\mathcal{P}$, $\mathcal{Q}$ stand for all discretized momentum variables (summation over repeated indices is implied). The matrix $\mathbf{K}=K^{i,\mathcal{P}}_{j,\mathcal{Q}}$ is the same in both equations, and subsumes the interaction kernel, the dressed propagators of the constituents, the Dirac- and Lorentz structure, as well as the discretized integrations. It is applied to a vector $F^{i,\mathcal{P}}$ representing the homogeneous or inhomogeneous amplitude.

As an alternative to the Nyström method, one can expand the momentum dependence of the components into suitable sets of orthogonal functions, which can then be integrated. In this approach, the index $\mathcal{P}$ of the vector $F^{i,\mathcal{P}}$ contains the coefficients of the expansion rather than the values of the components at certain points in momentum space (for applications in the present context, see e.g. [80,81]).

A partial application of this alternative is the use of a Chebyshev expansion of the dependence in an angle variable as described in Appendix A, where one only keeps a finite number of Chebyshev moments in the representation of the amplitude. This step has been widely used in DSE studies of hadron spectra and properties, and the fidelity of the approximation investigated in detail, see e.g. [46,82,83]. While for studies of hadron masses a few moments are sufficient, more are required in situations where considerable changes of the frame of reference are needed, such as form factor calculations at large momentum transfer [84]; ultimately, in these situations the approximation needs to be abandoned [55,85].

4. Solution methods

4.1. Homogeneous equations: eigenvalue algorithms

With the results of the preceding section, the homogeneous integral equation (BSE or Faddeev equation), given in Eq. (12) in index notation, can be written as

$$\vec{F}_{[h]}=\mathbf{K}\cdot\vec{F}_{[h]} \tag{14}$$

using matrix–vector notation. As already mentioned in Section 2, this equation is only valid at the on-shell points of the bound states in the respective channel, i.e. at certain values of the total momentum squared $P^2=-M_n^2$, where $n=0,1,2,\ldots$ numbers the ground- and all excited states in the channel. To find such a value of P^2, one investigates the spectrum of $\mathbf{K}$ as a function of

P^2, since Eq. (14) corresponds to an eigenvalue equation (with the dependence on P^2 made explicit)

$$\lambda(P^2)\vec{F}_{[h]}(P^2) = \mathbf{K}(P^2)\cdot\vec{F}_{[h]}(P^2), \tag{15}$$

where the eigenvalue $\lambda(P^2) = 1$. In other words, to numerically approach a solution of the equation, a part of the result has to be already known, namely the values M_n^2, or — more precisely — the mass of the state one is looking for. The way out is a self-consistency argument, where the eigenvalue spectrum is plotted as a function of P^2 and those points with $\lambda_n(P^2) = 1$ are identified: the largest eigenvalue determines the ground state, the smaller ones in succession the excitations of the system (see also Fig. 5 below).

Typically, one is interested in roughly up to five eigenvalues, since higher excitations are both not well-enough understood in theory and hard to access experimentally.

A great variety of algorithms is available to numerically tackle these kinds of problems, and the most commonly used is a simple iterative method. Similar to the other algorithms discussed here, it relies on the multiplication of the matrix $\mathbf{K}$ on a vector and can successively be applied to find also excited states, by projecting on states already obtained, see e.g. [86]. This simple method, however, is not able to resolve pairs of complex conjugate eigenvalues, which may, for example, occur in the meson BSE [87]. In addition, its convergence properties are not favorable, as demonstrated in Section 5.

Therefore, we recommend the use of more advanced algorithms which are able to overcome these difficulties. For this purpose, we utilize the implicitly restarted Arnoldi factorization [88], which is frequently applied in lattice QCD studies, e.g. [89]. An application of this algorithm to bound state calculations is demonstrated in Sections 5 and 6, where we use it to solve the homogeneous BSE and compare the efficiency of both methods.

4.2. Inhomogeneous equations: matrix inversion

In the most compact notation, the inhomogeneous integral equation can be written as

$$\vec{F}(P^2) = \vec{F}_0(P^2) + \mathbf{K}(P^2)\cdot\vec{F}(P^2) \tag{16}$$

where the matrix $\mathbf{K}(P^2)$ is identical to the one in Eq. (14), and the vector $\vec{F}_0$ is given by the decomposition of Γ_0 according to Eq. (7), $\Gamma_0 = \sum_i T_i F_0^i$ together with the discretization of a possible momentum dependence.

Again, the simplest method to treat this problem is a direct iteration. Mathematically, this corresponds to the representation of the solution by a von Neumann series (cf. [79, Chapter 4]), which can be shown to converge as long as the norm of the operator $\mathbf{K}$ is smaller than one, $\|\mathbf{K}\| < 1$. For matrices, this norm can be related to the largest eigenvalue, such that for $P^2 > -M_0^2$, the iteration converges. When P^2 approaches the ground state position $-M_0^2$ from above, the number of iterations necessarily grows, and no convergence is obtained if $P^2 \leqslant -M_0^2$, as demonstrated in Section 5.

However, a solution is possible for any P^2 if one rewrites Eq. (16) as

$$\vec{F} = (\mathbf{1} - \mathbf{K})^{-1}\cdot\vec{F}_0, \tag{17}$$

i.e., $\vec{F}$ is given by the inhomogeneous term $\vec{F}_0$ multiplied by the matrix inverse of $(\mathbf{1}-\mathbf{K})$. $\vec{F}$ can then be computed by e.g. inverting the matrix exactly, which has been successfully used to resolve bound-state poles in the inhomogeneous amplitude, as shown in [69] in the case of the quark–anti-quark system. On the downside, the direct inversion of a matrix is computationally expensive, and it is not straightforward to parallelize the procedure.

A better approach is to view Eq. (17) as a linear system whose solution is to be found. Equations like this are very common and several algorithms have been developed for their solution. In particular, if the matrix $(\mathbf{1}-\mathbf{K})$ is big, Eq. (17) is a typical application for the so-called Conjugate Gradient (CG) algorithms. Many types of these iterative Krylov-space methods are available. In the case of the bound-state equations considered here, the matrices involved are neither hermitian nor symmetric, such that a good choice is the well-known Bi-Conjugate-Gradients stabilized (BiCGstab) algorithm [90], which is widely used for example in lattice QCD (cf. [19, Chapter 6.2], where also the algorithm is presented in detail).

5. Illustration: numerical solution of the BSE

As an illustration, we apply the algorithms discussed above to solve the homogeneous and inhomogeneous pseudoscalar-meson BSEs and compare their efficiency in terms of the number of matrix–vector multiplications needed to achieve a specified accuracy. For bigger problems like baryons in a three-quark setup, the kernel matrix typically does not fit into memory, and thus has to be recomputed on the fly in each iteration- or matrix–vector multiplication step. In this case, one matrix–vector multiplication is rather time consuming and it is desirable to keep the number of necessary multiplications as small as possible.

For our test case here, however, we first study a quark–anti-quark system of pseudoscalar quantum numbers, where the kernel matrix is small, but one can still investigate the questions at hand — further quantum numbers are investigated in the following section. We employ the rainbow-ladder truncation, i.e. the rainbow approximation in the quark propagator DSE together with a ladder truncation of the corresponding quark–anti-quark BSE.

The quark self energy Σ in this truncation is given by

$$\Sigma = \frac{4}{3}\int_k \frac{\mathcal{D}(k)}{k^2} T^{\mu\nu}(k)\gamma_\mu S(k-q)\gamma_\nu, \tag{18}$$

where we define the transverse projector with respect to the momentum k as $T^{\mu\nu}(k) := (\delta_{\mu\nu} - \frac{k_\mu k_\nu}{k^2})$. Denoting the difference in relative momenta by $\ell := k - q$, the corresponding kernel $K_{[2]}(\gamma; k; q; P)$ of the BSEs, Eqs. (1) and (2), is then given by

$$K_{[2]}(\gamma; k; q; P) = -\frac{4}{3}\gamma_\mu \frac{\mathcal{D}(\ell^2)}{\ell^2} T^{\mu\nu}(\ell)\gamma_\nu, \tag{19}$$

where the effective interaction as a function of the momentum-squared s, introduced in Ref. [47], reads

$$\frac{\mathcal{D}(s)}{s} = D\left(\frac{4\pi^2}{\omega^6} s e^{-s/\omega^2}\right) + \mathcal{F}_{UV}(s). \tag{20}$$

The term $\mathcal{F}_{UV}(s)$ implements the perturbative running coupling of QCD for large s, preserving the one-loop renormalization-group behavior of QCD. The Gaussian term models the enhancement in the intermediate-momentum regime necessary to produce a reasonable amount of dynamical chiral symmetry breaking. It contains the parameters of the model, D and ω, describing the overall strength and momentum-space width (corresponding to an inverse effective range) of the interaction. The behavior of the effective interaction in the far infrared is expected to be of minor relevance to ground-state properties (cf. [91] and references therein). For the present study, we make a common choice for the parameters, namely $D = 0.93$ GeV^2 and $\omega = 0.4$ GeV (for full details on the truncation, the effective coupling, or the effects of other parameter values, see e.g. [39,46,47]).

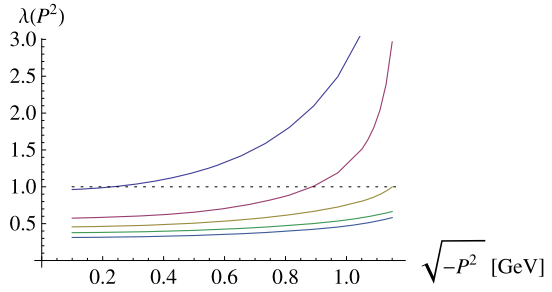

Fig. 5. The five largest eigenvalues of the homogeneous BSE plotted over $\sqrt{-P^2}$ which corresponds to the bound state mass M where $\lambda = 1$ indicated by the horizontal dashed line. The ground-state (leftmost intersection) solution vector has positive C-parity (pion), the second has negative (exotic) and the third again has positive C-parity (excited pion).

5.1. Kernel setup

The above definitions together with the dressed quark propagators computed already completely specify the ingredients of the BSE. We investigate light quarks in analogy to [39], where the current-quark mass in an isospin-symmetric setup was adjusted to fit the bound-state mass of the ρ meson. The details of the discretization of the kernel matrix proceed as follows: The orthonormal pseudoscalar covariants, constructed to satisfy Eq. (9), read

$$T_1 = \frac{\gamma_5}{2}, \tag{21}$$

$$T_2 = \frac{\gamma_5(\gamma\cdot P)}{2\sqrt{-P^2}}, \tag{22}$$

$$T_3 = \frac{\gamma_5((\gamma\cdot q) - \frac{(\gamma\cdot P)(P\cdot q)}{P^2})}{2\sqrt{\frac{(P\cdot q)^2}{P^2} - q^2}}, \tag{23}$$

$$T_4 = \frac{\frac{1}{2}i\gamma_5((\gamma\cdot q)(\gamma\cdot P) - (\gamma\cdot P)(\gamma\cdot q))}{2\sqrt{P^2q^2 - (P\cdot q)^2}}. \tag{24}$$

Choosing the rest frame of the quark–anti-quark system, and applying the parametrization and discretization as described in Appendix A, the kernel matrix Eq. (11) in our setup becomes

$$\begin{aligned}\mathbf{K} &= K^{i,r,s}_{j,l,m}(P) \\ &= -\frac{4}{3(2\pi)^3} w[q_l^2] w[z_m] \int_{-1}^{1} dy\, \frac{\mathcal{D}(\ell^2)}{\ell^2} T^{\mu\nu}(\ell) \\ &\quad \times \mathrm{Tr}\big[T_i(\gamma; k; P)\gamma_\mu S(q_+) T_j(\gamma; q; P) S(q_-)\gamma_\nu\big],\end{aligned} \tag{25}$$

where $w[q_l^2]$, $w[z_m]$ denote the quadrature weights and the replacements $k^2 \to k_r^2$, $z_k \to z_s$, $q^2 \to k_l^2$, $z \to z_m$ have been made in all occurring momenta to implement the discretization. Therefore, the indices $i; j$ label the components and $r, s; l, m$ the momentum space points. For the following calculations, we use $N_q = 32$ and $N_z = 24$, such that $\mathbf{K}$ has the dimensions $(32, 24, 4) \times (32, 24, 4)$.

5.2. Homogeneous BSE

To solve the homogeneous BSE, we use both the MPI based version of the ARPACK library (an implementation of the implicitly restarted Arnoldi factorization) and the simple iteration. Fig. 5 shows the largest five eigenvalues of $\mathbf{K}$ for our example. Bound-state masses can be identified by the positions at which an eigenvalue curve crosses one (dashed line in the figure) and from left to right correspond to the ground- and first-excited, second-excited, etc., states. Note that in our approach we do not restrict the symmetry of the amplitudes (eigenvectors) with respect to the angular variable z, such that we obtain homogeneous solutions of both positive and negative C-parity for equal-mass constituents and a choice of 1/2 for the momentum-partitioning parameters $\eta_\pm$, as indicated already above.

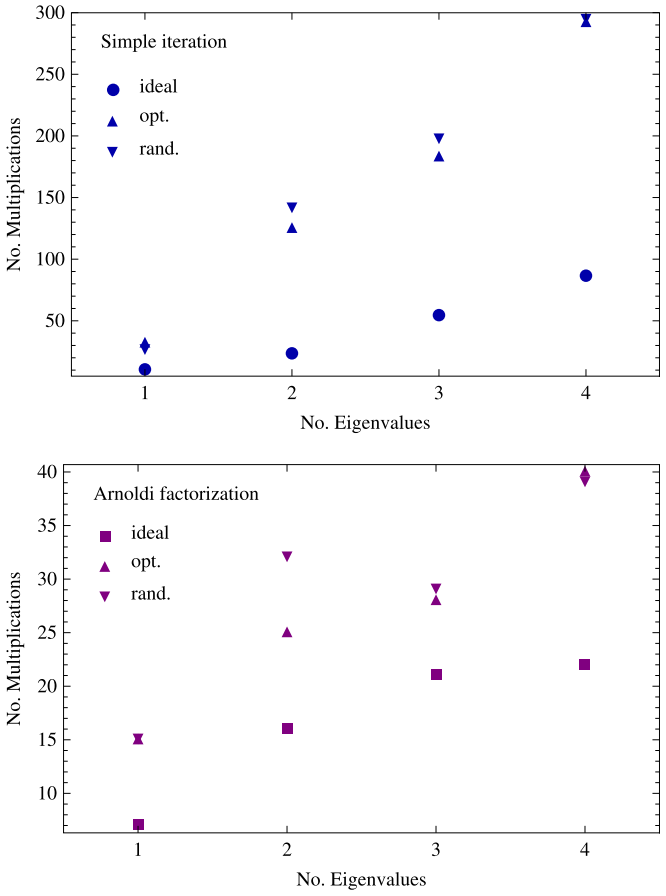

Fig. 6. The number of matrix–vector multiplications needed for convergence of the simple iteration (upper panel) and the Arnoldi factorization (lower panel), plotted against the number of eigenvalues computed at a (typical) fixed value of $P^2 = -M_0^2$ for random ("rand"), optimized ("opt"), and ideal initial conditions.

In the pseudoscalar case, a negative C-parity is considered *exotic*, since it is not available for a $\bar{q}q$ state in quantum mechanics. However, it appears naturally in a quark–anti-quark BSE setup, where our main interest here comes from a systematic point of view. A more general discussion of states with exotic C-parity in this formalism and their possible interpretations can be found, e.g., in [37,87,92,93].

To compare the efficiency of our algorithm of choice to solve the homogeneous BSE, the implicitly restarted Arnoldi factorization, to the standard method of simple iteration we compute the one to four largest eigenvalues of $\mathbf{K}$ and compare the convergence in terms of the number of iterations needed to obtain an accuracy of the eigenvector of $\epsilon = 10^{-8}$, at a (typical) value of $P^2 = -M_0^2 = 0.0527$ GeV^2. For the simple iteration, our stopping criterion demands that the absolute change in any element of the eigenvector from one iteration step to the next does not exceed the desired accuracy ϵ, while the vector is normalized to one with respect to the standard scalar product of $\mathbf{C}^n$, in order to be comparable to the ARPACK-library which works with the same scalar product. Note that the canonical normalization condition, Eq. (3), is applied subsequent to the eigenvalue calculation in order to compute physical observables.

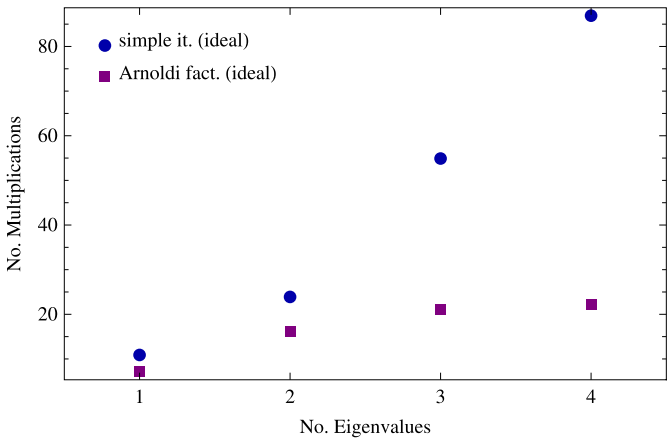

Fig. 7. The number of matrix–vector multiplications needed for convergence of the simple iteration (circles) and the Arnoldi factorization (squares), plotted against the number of eigenvalues computed at a (typical) fixed value of $P^2 = -M_0^2$, for ideal initial conditions.

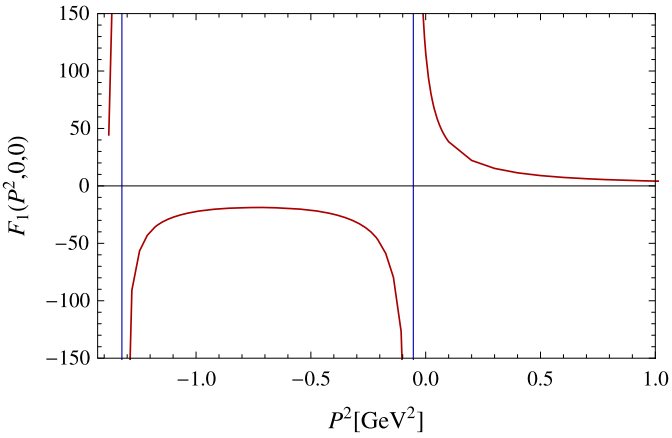

Fig. 8. Component $F_1(P^2, 0, 0)$ of the inhomogeneous pseudoscalar amplitude calculated using BiCGstab vs. the square of the total momentum P^2. The vertical lines mark the pole positions, corresponding to the pion ground- and first excited state ($J^{PC} = 0^{-+}$).

We compare three different initial conditions for both iterative procedures. First, we use the default settings provided by ARPACK, which are based on a random vector (cf. the ARPACK users guide [94]) opposed to a truly random initial vector $\vec{F}_{\text{in}}$ of complex numbers (where real and imaginary part are uniformly distributed in the interval $[0, 1]$) for the simple iteration. This choice is denoted by "rand". Second, we use optimized initial conditions which anticipate the UV behavior of the amplitudes as a simple power-law falloff while not imposing further symmetries by choosing

$$\vec{F}_{\text{in}} = \frac{(1+z)(1+\mathrm{i})}{1+q^2}, \tag{26}$$

which we denote by "opt". Third, we consider "ideal" initial conditions by utilizing the eigenvectors obtained at a nearby value of P^2, here $P^2 = -0.053361$ GeV^2, as $\vec{F}_{\text{in}}$. In ARPACK, if more than one eigenvalue is sought, the initial vector is set to the sum of the previously computed eigenvectors.

The results are given in Figs. 6 and 7, where the sensitivity of both algorithms to the initial conditions and the comparison of the efficiency in the ideal case are shown. From Fig. 6 it is clear that the Arnoldi factorization is less sensitive to a change in initial conditions than the simple iteration, and that it is in general more efficient. Even in the ideal case (cf. Fig. 7) for the first eigenvalue the advanced algorithm is 36% more efficient (7 iterations compared to 11), and becomes even more advantageous for an increasing number of eigenvalues.

Another interesting observation from Fig. 6 is that the Arnoldi factorization for random initial conditions was more efficient for three eigenvalues than when only two were requested. This is most likely due to a "clustering" of eigenvalues number two and three for the algorithm, an effect which appears for eigenvalues close together and is also related to the eigenvectors. In this particular case, eigenvectors two and tree have opposite C-parity or z-symmetry, which may make them more easily distinguishable for the algorithm and more easy to obtain as a result. The ARPACK library is very efficient at evaluating all eigenvalues in such a cluster, while convergence is slower if one asks for only one or a few of the eigenvalues in the cluster (cf. also [94]).

It should also be noted that the Arnoldi factorization requires, contrary to the simple iteration, already by construction a certain minimum of iterations, which depends on the parameters controlling the factorization, cf. [94].

5.3. Inhomogeneous BSE

We apply the direct iteration (summation of the von Neumann series) and the inversion using the BiCGstab algorithm to solve the inhomogeneous BSE (1), in the setup described above for pseudoscalar quantum numbers.

In the inhomogeneous case not only the structure of the amplitude determines the quantum numbers of the solution but also that of the inhomogeneous term Γ_0. Following [68], a possible choice for pseudoscalars is

$$\Gamma_0 = Z_4 \gamma_5, \tag{27}$$

where Z_4 is a renormalization constant obtained from the gap equation (cf. [46]). With this choice (pseudoscalar, positive C-parity), no poles corresponding to negative C-parity appear in the solution, as can be seen from Fig. 8. The curve shown in this figure has been obtained with the BiCGstab algorithm, because as described in Section 4.2 the direct iteration fails to converge if $P^2 \leqslant -M_0^2$.

This is demonstrated in Fig. 9, where the number of matrix–vector multiplications needed for convergence is plotted against P^2 for both methods. Here, we compare two choices of initial conditions: "ideal" starting values analogous to those discussed for the homogeneous equation, where the result of the calculation for the preceding value of P^2 (starting from $P^2 = 1$ GeV^2 in this case) is taken as initial guess, and the standard choice $\vec{F}_{\text{in}} = 0$. For both algorithms, the inversion was calculated to an accuracy of $\epsilon = 10^{-8}$, such that

$$\left\| \vec{F}_0 - (\mathbf{1} - \mathbf{K}) \cdot \vec{F}_{\text{fin}} \right\| \leqslant \epsilon,$$

where $\vec{F}_{\text{fin}}$ denotes the numerical result of the inversion, and the norm is a maximum-norm, which corresponds to the maximal absolute value of any element of the vector.

It is clear that, independent of the initial condition, the number of matrix–vector multiplications needed for the direct iteration diverges as P^2 approaches $-M_0^2$ (note that Fig. 9 uses a logarithmic scale on the vertical axis). The inversion with BiCGstab, however, converges for all P^2 with nearly the same speed, needing approximately 10 matrix–vector multiplications.

A further observation from Fig. 9 is that very close to the pole the standard initial conditions lead to faster convergence (by 1 iteration) than the ideal ones. This is most likely connected to the sign change in the components due to the pole, which is not taken into account in our definition of ideal initial conditions. In addition, these initial conditions also strongly depend on the step size.

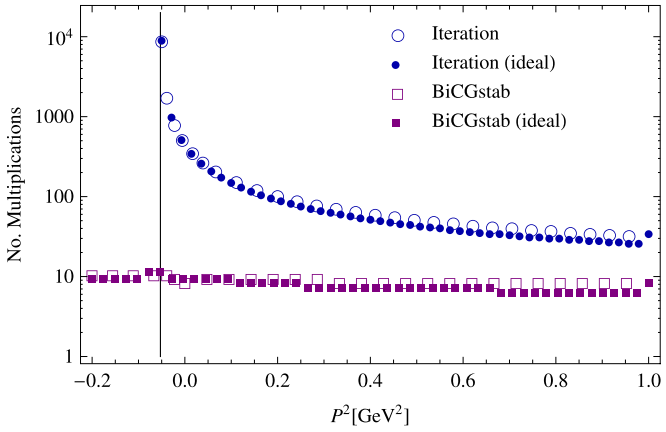

Fig. 9. The number of matrix–vector multiplications needed for convergence of the iterative solution of Eq. (1) (circles) and the BiCGstab algorithm (squares), plotted on a logarithmic scale against the square of the total momentum P^2 of the amplitude, for "ideal" initial conditions (full symbols) as well as for $F^j_{\text{in}} = 0$ (open symbols). The vertical line indicates the position of the ground state $P^2 = -M_0^2$ of the system. Note that the straightforward iteration does not converge for $P^2 \leqslant -M_0^2$.

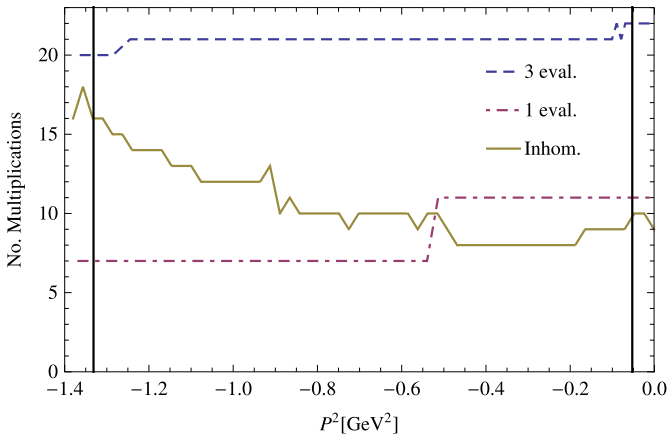

Fig. 10. The number of matrix–vector multiplications needed for convergence of the inhomogeneous BSE using BiCGstab (solid line) compared to the calculations of one eigenvalue (dash-dotted line) and three eigenvalues (dashed line) with the Arnoldi factorization. The vertical lines mark the ground and excited state in the 0^{-+} channel at $P_0^2 = -0.0527$ GeV^2 and $P_1^2 = -1.3315$ GeV^2.

As can be seen from Fig. 8, the inhomogeneous BSE can also be used to calculate the mass spectrum, such that it is interesting to compare the homogeneous and inhomogeneous equation directly in addition to the comparison of the solution methods of each equation.

We compare the matrix vector multiplications needed to solve the inhomogeneous BSE using the BiCGstab algorithm for a wide range of total momentum-squared to the solution of the eigenvalue problem for the homogeneous equation (using the Arnoldi factorization) in the same range for one and three eigenvalues. This calculation allows to obtain the masses of the pseudoscalar ground state and the first excitation for positive C-parity in our setup.

The results of the comparison are given in Fig. 10. Even though ideal initial conditions were used in all cases, the solution of the inhomogeneous BSE took less multiplications than the eigenvalue calculations in the region of the on-shell points of the ground state (corresponding to the first eigenvalue) and the first excitation (corresponding to the third eigenvalue), which are indicated by the vertical lines in the figure. This shows that in this case it is more efficient in terms of matrix–vector multiplications to use the inhomogeneous BSE to calculate the mass spectrum, especially the excited state.

In addition, following [45], the solution of the inhomogeneous vertex equation can also be used to calculate on-shell observables like decay constants, which are obtained as the residues of the corresponding projections of the inhomogeneous vertex BSA, such that the numerical advantages of the inhomogeneous vertex equation can be exploited in this case as well.

Demanding an even closer numerical correspondence, we have also tried to extract the entire homogeneous ground state amplitude from the inhomogeneous vertex BSA by fitting the residues in P^2 at each point of our relative-momentum-squared grid in a rather naive approach. While this appears possible in principle, the limiting factors in this case are the accuracies of the fit as well as the determination of the residues at the pole of the inhomogeneous vertex amplitude under investigation. In our pseudoscalar example, we were able to obtain the leading component of the homogeneous amplitude (which corresponds to the covariant T_1, Eq. (21)) with an accuracy of 2.6% when compared to the solution of the corresponding homogeneous BSE. The other components showed somewhat larger deviations such that this procedure cannot be performed without resorting to more involved fitting methods. Thus we conclude that, while obtaining the homogeneous BSA from the corresponding inhomogeneous vertex BSE is not impossible, with comparable numerical effort a determination directly from the homogeneous BSE is much more accurate.

6. Other quantum numbers

In order to check whether or not the results described above are limited to the special case of pseudoscalar quantum numbers, we discuss the application of the algorithms presented in this work to states with different parity and spin.

In the homogeneous case, we consider scalar, vector, axial-vector and tensor quantum numbers and use the same model and parameters as above in the pseudoscalar case. The bound states in these channels have been investigated thoroughly in [39] and recently [95], where all details concerning the parameter dependence and a comparison to experiment are given. The construction of orthonormal bases for these states is explained as well.

For the different quantum numbers, we compute the first eigenvalue (which on-shell corresponds to the ground state) for the four values of $J^{PC} = 0^{++}, 1^{--}, 1^{+-}, 2^{++}$ at a typical value of P^2 employing the Arnoldi factorization as well as the simple iteration, for both optimal and ideal initial conditions, as explained above. Note that the number of momentum-space points used for the integration is the same in all cases, while the number of covariants differs. For pseudoscalars and scalars, the basis consists of four covariants, while for the other quantum numbers eight covariants have to be used (see, e.g., [95]), which increases the size of the BSE kernel matrix.

The results, collected in Table 1, show that in each case the Arnoldi factorization was more efficient. Indeed, the advanced algorithm seems to be even more advantageous when applied to more complicated systems, which advocates its use also in studies of e.g. baryons.

Concerning the inhomogeneous BSE, it should be noted that the inversion using BiCGstab in any case is more efficient than the straightforward iteration, since one can prove (cf. Section 4.2) that this simple method does not converge beyond the first pole in the total momentum squared P^2.

Still, it is interesting to investigate the convergence of the inhomogeneous equation when compared to the homogeneous, in analogy to Fig. 10. The results for the 1^{--} channel are presented in Fig. 11. For the excited state, the advantages of the inhomogeneous equation are even more pronounced than for the

Table 1
Number of matrix–vector multiplications needed to achieve convergence of the Arnoldi factorization (Arn.) and the simple iteration (Iter.) when applied to the homogeneous BSE for the indicated quantum numbers (QN) J^{PC} at typical values of the total momentum squared P^2, for "optimized" and "ideal" initial conditions (with starting values computed at $-(\sqrt{-P^2}-0.01)^2$ in each case).

Initial conditions:		Optimal		Ideal	
QN	P^2 [GeV^2]	Arn.	Iter.	Arn.	Iter.
0^{++}	−0.509796	15	40	10	15
1^{--}	−0.599695	15	74	10	31
1^{+-}	−0.739772	20	103	10	15
2^{++}	−1.254400	20	63	15	46

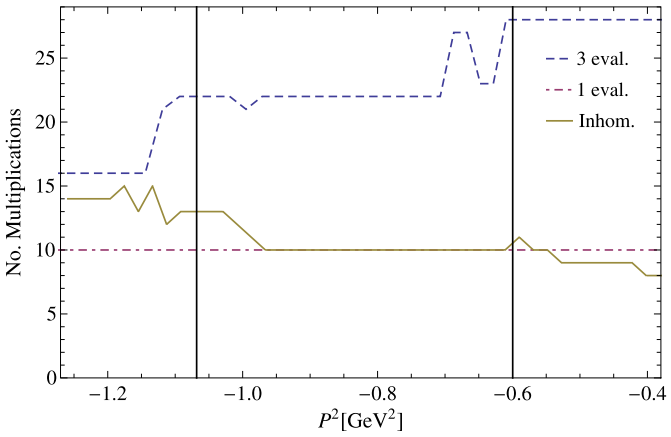

Fig. 11. The number of matrix–vector multiplications needed for convergence of the inhomogeneous BSE using BiCGstab (solid line) compared to the calculations of one eigenvalue (dash-dotted line) and three eigenvalues (dashed line) with the Arnoldi factorization. The vertical lines mark the ground and excited state in the 1^{--} channel at $P_0^2 = -0.5997$ GeV^2 and $P_1^2 = -1.0682$ GeV^2.

pseudoscalar channel, whereas for the ground state the two equations are almost equivalent in terms of efficiency.

7. Conclusion and outlook

We have investigated the applicability of well-known and efficient matrix algorithms to homogeneous and inhomogeneous covariant bound state and vertex equations. In a fully numerical setup, a homogeneous bound state equation such as the BSE or Faddeev equation can be solved as an eigenvalue problem, and its inhomogeneous counterpart as a linear system. For their solution, we employ the implicitly restarted Arnoldi factorization and the stabilized Bi-Conjugate Gradient algorithm.

As an illustration, we studied the homogeneous and inhomogeneous BSE, where we have shown that these algorithms are more efficient than the standard methods applied usually in this context. Furthermore, we find that for the calculation of the mass spectrum (and consequently also for decay constants, cf. [45]) it is as efficient or even advantageous to use the inhomogeneous instead of the homogeneous equation, especially when considering excitations. This is valuable insight which is worth considering in particular for studies of baryons in a three-quark setup and more involved systems.

In addition, due to their iterative nature, the algorithms employed are straightforwardly parallelizable and can thus be used effectively on CPU and GPU clusters. Especially bound state problems involving more than two constituents, starting with but not limited to baryons in a three-quark setup, need efficient methods to perform sophisticated numerical studies. The typical size of the kernel matrices appearing in such systems exceeds by far the storage capacity of present-day computing infrastructure, and thus only certain parts can be stored. The elements of the matrix have to be computed on the fly when needed, such that the amount of memory actually required for such a calculation is rather small. Therefore, these problems are not memory- but CPU-bound and thus appear to be ideal applications for the field of GPU computing.

Acknowledgements

We would like to acknowledge valuable discussions with R. Alkofer, C.S. Fischer, C. Gattringer, C.B. Lang, A. Maas, D. Mohler, C.D. Roberts, M. Schwinzerl, and S.V. Wright. This work was supported by the Austrian Science Fund *FWF* under project No. P20496-N16, and was performed in association with and supported in part by the *FWF* doctoral program No. W1203-N08.

Appendix A. Aspects of four-dimensional momentum integration

We use 4-dim. spherical coordinates, such that the momentum integration is written as

$$\int_{-\infty}^{\infty} d^4q \to \int_0^{\infty} d(q^2)\,\frac{q^2}{2}\int_{-1}^{1} dz\sqrt{1-z^2}\int_{-1}^{1} dy\int_0^{2\pi} d\phi. \tag{A.1}$$

In the meson BSE, there are three relevant momenta: P (total momentum), k (relative momentum), and q (loop momentum). Subsequently, we choose P to be in the rest-frame of the bound state,

$$P = \left(0,0,0,\sqrt{P^2}\right). \tag{A.2}$$

The other momenta are chosen accordingly and read

$$k = \sqrt{k^2}\left(0,0,\sqrt{1-z_k^2},z_k\right) \tag{A.3}$$

and

$$q = \sqrt{q^2}\left(0,\sqrt{1-z^2}\sqrt{1-y^2},\sqrt{1-z^2}y,z\right). \tag{A.4}$$

In this parametrization, the integration $\int d\phi$ is trivial.

The components of the amplitude on the left-hand side of the BSEs Eqs. (1) and (2) depend on the scalar products $P\cdot k = z_k\sqrt{k^2}\sqrt{P^2}$, P^2, and k^2. Inside the integral, on the right-hand side, the scalar products become $P\cdot q = z\sqrt{q^2}\sqrt{P^2}$, P^2, and q^2. Thus, the BSE kernel matrix **K** induces the following mapping on the momentum variables

$$\left(q^2,z\right)\mapsto\left(k^2,z_k\right), \tag{A.5}$$

such that the integration $\int dy$ does not add a dimension **K**, although it is not trivial.

After choosing a parametrization of the momentum integration, the next step is to discretize the momentum dependence. In this work, we straightforwardly apply the quadrature method, and replace

$$\int_0^{\infty} d(q^2)\,\frac{q^2}{2}\int_{-1}^{1} dz\sqrt{1-z^2} \to \sum_{l=1}^{N_q}\sum_{m=1}^{N_z} w\left[q_l^2\right]w[z_m], \tag{A.6}$$

where $w[q_l^2]$, $w[z_m^2]$ denote the quadrature weights and q_l^2, z_m the corresponding nodes. The factors of $q^2/2$ and $\sqrt{1-z^2}$ have been absorbed in the weights.

Note that, especially for the integration over z, it is advantageous to use a quadrature rule whose weights include $\sqrt{1-z^2}$ by construction, e.g., the Gauss–Chebyshev type 2 rule.

An alternative, advantageous and widely used in the calculations of hadron spectra is to apply the quadrature method discussed above only to $\int d(q^2)$ and to resolve the z-dependence and

by an expansion in Chebyshev polynomials of the second kind. The components are then written as

$$F^i(P^2, q^2, z) = \sum_{m=1}^{M} {}^m F_i(q^2, P^2) U_m(z), \tag{A.7}$$

with ${}^m F_i(q^2, P^2)$ the so-called Chebyshev *moments*, which retain only the functional dependence on k^2 and P^2. The number of terms M taken into account is finite in practice, but infinite in principle. The Chebyshev polynomials of the second kind $U_m(z)$ satisfy the orthogonality relation

$$\frac{2}{\pi} \int dz \sqrt{1-z^2} U_m(z) U_n(z) = \delta_{mn}. \tag{A.8}$$

To obtain a matrix structure not only in the covariants, but also in the Chebyshev moments, the above expansion is inserted in Eq. (11), and is then projected on one moment by use of Eq. (A.8). This finally leads to

$$\begin{aligned} &\int_q K^{i,m}_{j,n}(k; q; P)\, {}^n F_j(q^2, P^2) \\ &= \left(\frac{2}{\pi} \int_q \int_{-1}^{1} dz_k\, U_m(z_k) \mathrm{Tr}\big[T_i(\gamma; k; P) K_{[2]}(\gamma; k; q; P) \right. \\ &\quad \left. \times S^a(\gamma; q; P) T_j(\gamma; q; P) S^b(\gamma; q; P) \big] U_n(z) \right) {}^n F_j(q^2, P^2). \end{aligned} \tag{A.9}$$

Again, the sum over the repeated indices j, n is implied.

Appendix B. Using a non-orthogonal Dirac basis

Consider the inhomogeneous BSE written in the general form

$$\begin{aligned} &f(\gamma; k; P) \Gamma(\gamma; k; P) \\ &\quad = Z(\gamma; k; P) - \int_q K_1(\gamma; k; q; P) \Gamma(\gamma; q; P) K_2(\gamma; k; q; P), \end{aligned} \tag{B.1}$$

where the dependence of every term on all variables including γ matrices is given explicitly. The ; between variables again denotes a dependence on complete four-vectors. K_1 and K_2 represent generalized formal kernel pieces, Z a general driving term, and f an arbitrary function of its arguments. To transform this equation into a set of coupled integral equations for components and then use Chebyshev moments, which are described in Appendix A, we write the BSA as the sum over its covariants T_i and Lorentz- as well as Dirac-scalar components F^i and the latter as sums over Chebyshev polynomials and moments

$$\Gamma(\gamma; k; P) = \sum_{i=1}^{M} \sum_{j=1}^{N} T_j(\gamma; k; P)\, {}^i F_j(k^2, P^2) U_i(z_k), \tag{B.2}$$

where M is the number of Chebyshev polynomials taken into account and N is the number of covariants in the BSA. The Chebyshev polynomial of the second kind $U_i(z_k)$ depends on $z_k := k \cdot P / \sqrt{k^2 P^2}$. Now we apply $T_n(\gamma; k; P)$ on Eq. (B.1) from the left and take the Dirac trace. The result is

$$\begin{aligned} &\sum_{i=1}^{M} \sum_{j=1}^{N} A_{nj}(k^2, P^2, z_k)\, {}^i F_j(k^2, P^2) U_i(z_k) \\ &\quad = Z_n(k^2, P^2, z_k) - \sum_{l=1}^{M} \sum_{m=1}^{N} \int_q \mathrm{Tr}\big[T_n(\gamma; k; P) \\ &\qquad \times K_1(\gamma; k; q; P) T_m(\gamma; q; P)\, {}^l F_m(q^2, P^2) \\ &\qquad \times U_l(z_q) K_2(\gamma; k; q; P) \big], \end{aligned} \tag{B.3}$$

where

$$\begin{aligned} A_{nj}(k^2, P^2, z_k) &:= \mathrm{Tr}\big[T_n(\gamma; k; P) f(\gamma; k; P) T_j(\gamma; k; P) \big], \\ Z_n(k^2, P^2, z_k) &:= \mathrm{Tr}\big[T_n(\gamma; k; P) Z(\gamma; k; P) \big]. \end{aligned} \tag{B.4}$$

The next step is to invert the matrix A_{nj} for each set of coordinates (k^2, P^2, z_k), and apply its inverse to the equation, i.e., $\sum_{n=1}^{N} A^{-1}_{rn}$ from the left:

$$\begin{aligned} &\sum_{i=1}^{M} {}^i F_r(k^2, P^2) U_i(z_k) \\ &\quad = \sum_{n=1}^{N} A^{-1}_{rn}(k^2, P^2, z_k) Z_n(k^2, P^2, z_k) \\ &\qquad - \sum_{n=1}^{N} \sum_{l=1}^{M} \sum_{m=1}^{N} \int_q A^{-1}_{rn}(k^2, P^2, z_k) \\ &\qquad \times \mathrm{Tr}\big[T_n(\gamma; k; P) K_1(\gamma; k; q; P) T_m(\gamma; q; P) \\ &\qquad \times {}^l F_m(q^2, P^2) U_l(z_q) K_2(\gamma; k; q; P) \big]. \end{aligned} \tag{B.5}$$

The last step is the projection with the help of Chebyshev polynomials via $\frac{2}{\pi} \int dz_k \sqrt{1-z_k^2} U_j(z_k)$ from the left (cf. Eq. (A.8)) and one obtains

$$\begin{aligned} &{}^j F_r(k^2, P^2) \\ &\quad = V_Z(j, r, k^2) - \sum_{l=1}^{M} \sum_{n,m=1}^{N} \frac{2}{\pi} \int_q \int_{z_k} \sqrt{1-z_k^2} \\ &\qquad \times U_j(z_k) A^{-1}_{rn}(k^2, P^2, z_k) \mathrm{Tr}\big[T_n(\gamma; k; P) K_1(\gamma; k; q; P) \\ &\qquad \times T_m(\gamma; q; P)\, {}^l F_m(q^2, P^2) U_l(z_q) K_2(\gamma; k; q; P) \big] \end{aligned} \tag{B.6}$$

with the driving term given by

$$\begin{aligned} V_Z(j, r, k^2) &:= \frac{2}{\pi} \sum_{n=1}^{N} \int dz_k \sqrt{1-z_k^2} U_j(z_k) \\ &\quad \times A^{-1}_{rn}(k^2, P^2, z_k) Z_n(k^2, P^2, z_k). \end{aligned} \tag{B.7}$$

This procedure does not require the set of covariants to be orthogonal, it is completely general, also with respect to the kernel, the driving term, and possible terms multiplying the amplitude on the left-hand side of the BSE. All terms and projections are included correctly via the matrix A. In the case considered in the present work, $f = 1$ and the driving term has the standard form for pseudoscalar mesons, Eq. (27).

References

[1] W.J. Marciano, H. Pagels, Phys. Rept. 36 (1978) 137.
[2] D.J. Gross, F. Wilczek, Phys. Rev. Lett. 30 (1973) 1343–1346.
[3] D.J. Gross, F. Wilczek, Phys. Rev. D 8 (10) (1973) 3633–3652.
[4] H.D. Politzer, Phys. Rev. Lett. 30 (1973) 1346–1349.
[5] G.P. Lepage, S.J. Brodsky, Phys. Rev. D 22 (1980) 2157.
[6] S. Godfrey, N. Isgur, Phys. Rev. D 32 (1985) 189–231.
[7] S. Capstick, N. Isgur, Phys. Rev. D 34 (1986) 2809.
[8] L.Y. Glozman, W. Plessas, K. Varga, R.F. Wagenbrunn, Phys. Rev. D 58 (1998) 094030.

[9] T. Barnes, S. Godfrey, E.S. Swanson, Phys. Rev. D 72 (2005) 054026.
[10] T. Melde, W. Plessas, B. Sengl, Phys. Rev. D 77 (2008) 114002.
[11] J. Gasser, H. Leutwyler, Ann. Phys. 158 (1984) 142.
[12] S. Scherer, Adv. Nucl. Phys. 27 (2003) 277.
[13] N. Brambilla, et al., arXiv:hep-ph/0412158.
[14] C. McNeile, C. Michael, Phys. Rev. D 74 (2006) 014508.
[15] T. Burch, et al., Phys. Rev. D 73 (2006) 094505.
[16] H. Wada, et al., Phys. Lett. B 652 (2007) 250–254.
[17] J.J. Dudek, R.G. Edwards, N. Mathur, D.G. Richards, Phys. Rev. D 77 (2008) 034501.
[18] E.B. Gregory, A.C. Irving, C. McNeile, C. Richards, PoS Lattice2008 (2009) 286.
[19] C. Gattringer, C.B. Lang, Lect. Notes Phys. 788 (2010) 1–211.
[20] P. Colangelo, A. Khodjamirian, arXiv:hep-ph/0010175.
[21] M. Jamin, B.O. Lange, Phys. Rev. D 65 (2002) 056005.
[22] K. Maltman, J. Kambor, Phys. Rev. D 65 (2002) 074013.
[23] A.A. Penin, M. Steinhauser, Phys. Rev. D 65 (2002) 054006.
[24] P. Ball, R. Zwicky, Phys. Rev. D 71 (2005) 014015.
[25] W. Lucha, D. Melikhov, H. Sazdjian, S. Simula, Phys. Rev. D 80 (2009) 114028.
[26] H. Gies, C. Wetterich, Phys. Rev. D 65 (2002) 065001.
[27] J.M. Pawlowski, Annals Phys. 322 (2007) 2831–2915.
[28] R. Alkofer, J. Greensite, J. Phys. G 34 (2007) S3.
[29] C.D. Roberts, A.G. Williams, Prog. Part. Nucl. Phys. 33 (1994) 477–575.
[30] R. Alkofer, L. von Smekal, Phys. Rept. 353 (2001) 281.
[31] C.S. Fischer, J. Phys. G 32 (2006) R253–R291.
[32] P. Maris, C.D. Roberts, Int. J. Mod. Phys. E 12 (2003) 297–365.
[33] C.D. Roberts, M.S. Bhagwat, A. Holl, S.V. Wright, Eur. Phys. J. Special Topics 140 (2007) 53–116.
[34] C.D. Roberts, S.M. Schmidt, Prog. Part. Nucl. Phys. 45 (2000) S1–S103.
[35] H.A. Bethe, E.E. Salpeter, Phys. Rev. 82 (1951) 309.
[36] E.E. Salpeter, H.A. Bethe, Phys. Rev. 84 (1951) 1232–1242.
[37] C.H. Llewellyn-Smith, Ann. Phys. 53 (1969) 521–558.
[38] P. Jain, H.J. Munczek, Phys. Rev. D 48 (1993) 5403–5411.
[39] A. Krassnigg, Phys. Rev. D 80 (2009) 114010.
[40] L.D. Faddeev, Sov. Phys. JETP 12 (1961) 1014–1019.
[41] V.A. Karmanov, P. Maris, Few-Body Syst. 46 (2009) 95–113.
[42] G. Eichmann, R. Alkofer, A. Krassnigg, D. Nicmorus, Phys. Rev. Lett. 104 (2010) 201601.
[43] R. Alkofer, C.S. Fischer, F.J. Llanes-Estrada, K. Schwenzer, Annals Phys. 324 (2009) 106.
[44] C.S. Fischer, A. Maas, J.M. Pawlowski, Annals Phys. 324 (2008) 2408–2437.
[45] M. Blank, A. Krassnigg, arXiv:1011.5772.
[46] P. Maris, C.D. Roberts, Phys. Rev. C 56 (1997) 3369–3383.
[47] P. Maris, P.C. Tandy, Phys. Rev. C 60 (1999) 055214.
[48] M.A. Ivanov, Y.L. Kalinovsky, C.D. Roberts, Phys. Rev. D 60 (1999) 034018.
[49] D. Jarecke, P. Maris, P.C. Tandy, Phys. Rev. C 67 (2003) 035202.
[50] D.W. Jarecke, Properties of mesons from Bethe–Salpeter amplitudes, Ph.D. thesis, Kent State University, 2005.
[51] M.A. Ivanov, Y.L. Kalinovsky, P. Maris, C.D. Roberts, Phys. Rev. C 57 (1998) 1991–2003.
[52] P. Maris, P.C. Tandy, Phys. Rev. C 61 (2000) 045202.
[53] P. Maris, P.C. Tandy, Phys. Rev. C 62 (2000) 055204.
[54] A. Holl, A. Krassnigg, P. Maris, C.D. Roberts, S.V. Wright, Phys. Rev. C 71 (2005) 065204.
[55] M.S. Bhagwat, P. Maris, Phys. Rev. C 77 (2008) 025203.
[56] M. Oettel, R. Alkofer, Eur. Phys. J. A 16 (2003) 95–109.
[57] R. Alkofer, A. Holl, M. Kloker, A. Krassnigg, C.D. Roberts, Few-Body Syst. 37 (2005) 1–31.
[58] G. Eichmann, A. Krassnigg, M. Schwinzerl, R. Alkofer, Annals Phys. 323 (2008) 2505–2553.
[59] R. Alkofer, G. Eichmann, A. Krassnigg, D. Nicmorus, Chinese Physics C 34 (2010) 1175–1180.
[60] D. Nicmorus, G. Eichmann, R. Alkofer, arXiv:1008.3184.
[61] D. Nicmorus, G. Eichmann, A. Krassnigg, R. Alkofer, arXiv:1008.4149.
[62] P. Watson, W. Cassing, Few-Body Syst. 35 (2004) 99–115.
[63] P. Watson, W. Cassing, P.C. Tandy, Few-Body Syst. 35 (2004) 129–153.
[64] C.S. Fischer, R. Williams, Phys. Rev. D 78 (2008) 074006.
[65] C.S. Fischer, R. Williams, Phys. Rev. Lett. 103 (2009) 122001.
[66] L. Chang, C.D. Roberts, Phys. Rev. Lett. 103 (2009) 081601.
[67] L. Chang, C.D. Roberts, AIP Conf. Proc. 1261 (2010) 25–30.
[68] P. Maris, C.D. Roberts, P.C. Tandy, Phys. Lett. B 420 (1998) 267–273.
[69] M.S. Bhagwat, A. Hoell, A. Krassnigg, C.D. Roberts, S.V. Wright, Few-Body Syst. 40 (2007) 209–235.
[70] G. Eichmann, R. Alkofer, A. Krassnigg, D. Nicmorus, EPJ Web of Conferences 3 (2010) 03028.
[71] G. Eichmann, Hadron properties from QCD bound-state equations, Ph.D. thesis, University of Graz, 2009.
[72] A. Holl, A. Krassnigg, C.D. Roberts, Phys. Rev. C 70 (2004) 042203(R).
[73] H.J. Munczek, Phys. Rev. D 52 (1995) 4736–4740.
[74] A. Bender, C.D. Roberts, L. Von Smekal, Phys. Lett. B 380 (1996) 7–12.
[75] M.S. Bhagwat, A. Holl, A. Krassnigg, C.D. Roberts, P.C. Tandy, Phys. Rev. C 70 (2004) 035205.
[76] C.S. Fischer, P. Watson, W. Cassing, Phys. Rev. D 72 (2005) 094025.
[77] C.S. Fischer, D. Nickel, R. Williams, Eur. Phys. J. C 60 (2008) 1434–6052.
[78] A. Krassnigg, PoS Confinement 8 (2009) 75.
[79] L.M. Delves, J.L. Mohamed, Computational Methods for Integral Equations, Cambridge University Press, 1985.
[80] M.S. Bhagwat, M.A. Pichowsky, P.C. Tandy, Phys. Rev. D 67 (2003) 054019.
[81] S.M. Dorkin, T. Hilger, L.P. Kaptari, B. Kaempfer, arXiv:1008.2135.
[82] M. Oettel, L. Von Smekal, R. Alkofer, Comput. Phys. Commun. 144 (2002) 63.
[83] R. Alkofer, P. Watson, H. Weigel, Phys. Rev. D 65 (2002) 094026.
[84] A. Höll, R. Alkofer, M. Kloker, A. Krassnigg, C.D. Roberts, S.V. Wright, Nucl. Phys. A 755 (2005) 298–302.
[85] P. Maris, P.C. Tandy, Nucl. Phys. Proc. Suppl. 161 (2006) 136–152.
[86] A. Krassnigg, C.D. Roberts, Fizika B 13 (2004) 143–152.
[87] S. Ahlig, R. Alkofer, Annals Phys. 275 (1999) 113–147.
[88] D.C. Sorensen, Implicitly restarted Arnoldi/Lanczos methods for large scale eigenvalue calculations, Tech. Rep. TR-96-40, Rice University, Houston, Texas, 1996, citeseer.ist.psu.edu/174335.html.
[89] M. Joergler, C.B. Lang, PoS LAT 2007 (2007) 107.
[90] H.A. van der Vorst, SIAM J. Sci. Stat. Comput. 13 (2) (1992) 631–644.
[91] M. Blank, A. Krassnigg, A. Maas, Phys. Rev. D 83 (2011) 034020, arXiv:1007.3901.
[92] N. Nakanishi, Prog. Theor. Phys. Suppl. 43 (1969) 1–81.
[93] C.J. Burden, M.A. Pichowsky, Few-Body Syst. 32 (2002) 119–126.
[94] R.B. Lehoucq, D.C. Sorensen, C. Yang, ARPACK Users' Guide: Solution of Large-Scale Eigenvalue Problems with Implicitly Restarted Arnoldi Methods, Society for Industrial & Applied Mathematics, 1998.
[95] A. Krassnigg, M. Blank, arXiv:1011.6650.